EPJ manuscript No.
(will be inserted by the editor)

Isomers of astrophysical interest in neutron-deficient nuclei at masses A = 81, 85 and 86

A. Kankainen[1], G.K. Vorobjev[2,3a], S.A. Eliseev[3,4], W. Huang[1], J. Huikari[1], A. Jokinen[1], A. Nieminen[1], Yu.N. Novikov[2,3], H. Penttilä[1], A.V. Popov[3], S. Rinta-Antila[1], H. Schatz[5], D.M. Seliverstov[3], Yu.P. Suslov[2], and J. Äystö[1]

[1] Department of Physics, P.O. Box 35, FIN-40014 University of Jyväskylä, Finland
[2] St. Petersburg State University, St. Petersburg 198904, Russia
[3] Petersburg Nuclear Physics Institute, 188300 Gatchina, St. Petersburg, Russia
[4] GSI, Postfach 110552, D-64291 Darmstadt, Germany
[5] Michigan State University, East Lansing, MI 48824, USA

Received: date / Revised version: date

Abstract. Decay properties of neutron-deficient exotic nuclei close to $A = 80$ have been investigated at the IGISOL facility. The studied nuclei, ^{81}Y, ^{81}Sr, ^{81m}Kr, ^{85}Nb, ^{85}Zr, ^{86}Mo and ^{86}Nb, were produced by a ^{32}S beam from the Jyväskylä isochronous cyclotron on ^{54}Fe and ^{nat}Ni targets. The internal conversion coefficient for a 190.5 keV isomeric transition in ^{81m}Kr has been measured and the internal transition rate has been determined. The internal transition rate has been used to estimate a neutrino capture rate on ^{81}Br, which yields a log *ft* of 5.13 ± 0.09 for the reaction $^{81}\mathrm{Br}(\nu, e^-)^{81m}\mathrm{Kr}$. A new isomer with a half-life of 3.3 ± 0.9 s has been observed in ^{85}Nb. The existence of an earlier reported isomer with a half-life of 56 s in ^{86}Nb has not been confirmed.

PACS. 21.10.Tg Lifetimes – 23.20.Nx Internal conversion and extranuclear effects – 27.50.+e $59 \leq A \leq 89$

1 Introduction

Nuclei close to the $N = Z$ line in the region near $A = 80$ play a special role in nuclear astrophysics since the rapid proton (rp) capture process is passing right through them (see fig. 1). The rp-process, a sequence of rapid proton captures and β^+ decays, proceeds along the $N = Z$ line up to ^{56}Ni and it can continue ending in a SnSbTe cycle either in explosive X-ray bursts or in steady state burning (*e.g.*, in X-ray pulsars) [1,2]. At higher Z values, where proton capture rates become smaller, the reaction path can be broader and shifted by about one or two mass units towards the beta-stability line [1]. This shift can be even greater for the steady state burning model [2].

The properties of neutron-deficient nuclei involved in the rp-process, especially masses and beta-decay half-lives, are needed to perform rp-process nuclear reaction network calculations. These simulations are crucial for the understanding of the energy generation and fuel consumption in the rp-process and its potential contribution to galactic nucleosynthesis [1]. The discovery of new long-lived isomeric states in neutron-deficient nuclei is of potential importance for rp-process calculations. Low-lying excited states are thermally populated at the high astrophysical temperatures and densities. The contribution from such excited states can therefore alter proton capture rates and β^+/EC decay rates considerably and introduce an additional temperature dependence for those rates. This is particularly true for isomeric states. Such states typically have different properties than the ground state and

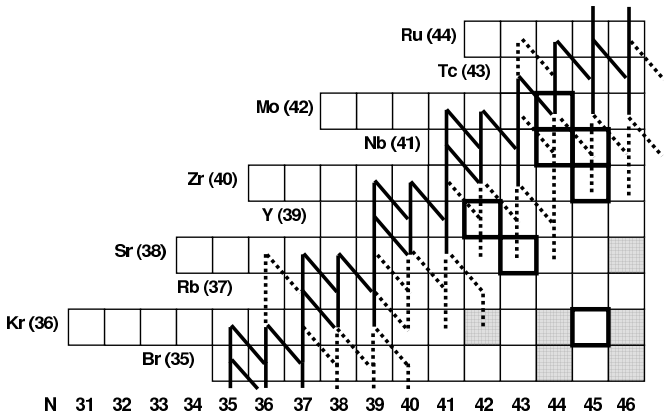

Fig. 1. The rp-process path close to $A = 80$ for steady state burning taken from ref. [2]. The reaction flow of more than 10 % is shown by the solid line and of 1–10 % by the dashed line. The nuclei studied in this work are highlighted by squares.

[a] *Present address:* GSI, Postfach 110552, D-64291 Darmstadt, Germany

therefore potentially different capture and decay rates. In addition, if there is no path for rapid thermalisation at rp-process temperatures, the relative population of the isomeric state can exceed by far the usually small thermal population. However, spectroscopic information on rp-process nuclei is still scarce, particularly for nuclides around $A = 80$. The success in our previous experiment done at $A = 80$ [3] encouraged us to continue studies in this field. In this work we have focused on the properties of isomeric states and on the search for new isomers.

Another problem in astrophysics directly related to our present study is solar neutrino detection. After the experiment using the ^{37}Cl detector [4] had shown the discrepancy between expected and experimental solar neutrino fluxes, it was suggested that the flux should be measured for lower neutrino energies. For this purpose other detectors were proposed, one of which was based on ^{81}Br [5]. Although the solar neutrino flux puzzle has recently been explained by neutrino oscillations, more solar neutrino experiments are required to measure the CNO fusion cycle contribution in the solar luminosity and new types of detectors are very desirable. According to current solar model calculations, 98.5 % of the solar luminosity is provided by the p-p chain and only 1.5 % by CNO reactions. At the moment, solar neutrino experiments have only set an upper limit of 7.8 % to the CNO fraction of the Sun's luminosity [6].

The threshold energy for neutrino capture in the proposed ^{81}Br detector is a factor of two lower than in ^{37}Cl (see fig. 2). It is assumed that a ^{81}Br detector is most sensitive to ^{8}B neutrinos [7] but ^{7}Be neutrinos as well as neutrinos from ^{13}N and ^{15}O decays from the CNO cycle can also contribute. In radiochemical experiments ^{81}Br can be used for total solar neutrino flux measurements because its energy threshold allows the observation of neutrino-induced events from all main solar neutrino sources mentioned above. In addition, ^{81}Br serves as a possible isotope to determine the average integrated flux over the past 300 000 years from neutrino produced ^{81}Kr concentration in minerals containing bromine [5]. Meanwhile, a detailed investigation of Gamow-Teller and Fermi transition strengths for all allowed transitions from ^{81}Br to the states below the particle emission threshold in ^{81}Kr is needed to calculate contributions of different neutrino components [7].

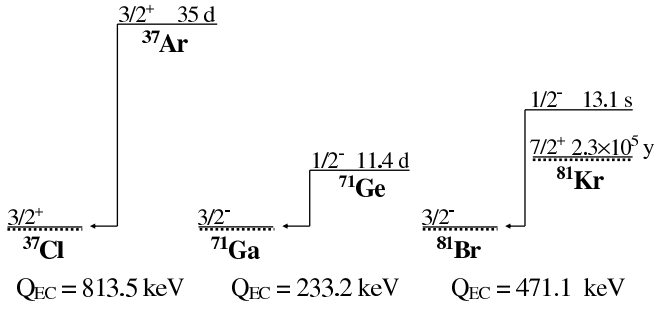

Fig. 2. Isotopes proposed for solar neutrino detectors.

In order to obtain the neutrino capture cross section on ^{81}Br, the probability for the inverse process of electron capture decay of ^{81}Kr must be measured. As can be seen from fig. 3, the neutrino capture on ^{81}Br should predominantly populate the isomeric state at 190.5 keV in ^{81}Kr because this allowed transition has to be six orders of magnitude stronger than the capture to the ground state of ^{81}Kr, whose inverse rate is well known [8]. Thus, the rates for all decay branches of ^{81m}Kr, which are electron capture, internal conversion and γ-decay, are needed to derive the electron capture probability. The data for the K-electron capture channel, determined independently by two groups [9,10], are in satisfactory agreement but the information on the internal transition (γ- and conversion electron branches) is strongly contradictory. Therefore, the electron capture branching ratio has not been obtained with high accuracy and new measurements on the internal decay channel of ^{81m}Kr are needed.

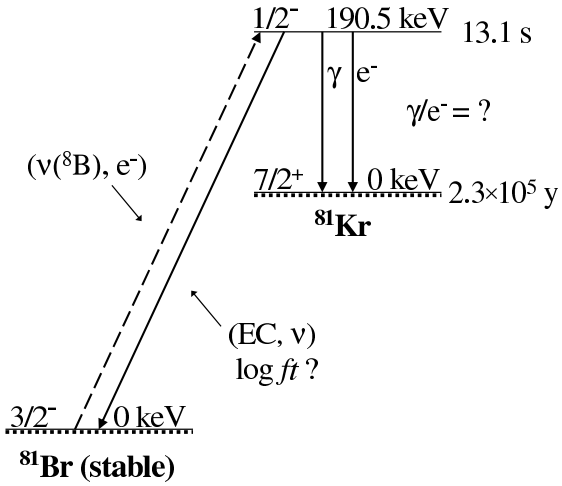

Fig. 3. A decay scheme of the isomeric state ^{81m}Kr (13.1 s).

2 Experimental method

The experiment was performed using the IGISOL facility at the Jyväskylä isochronous cyclotron. The isotopes of interest were produced by a 150–170 MeV $^{32}S^{7+}$ beam with an intensity of about 500 nA on ^{nat}Ni (2 mg/cm^2) and ^{54}Fe (1.8 mg/cm^2) targets. The ^{nat}Ni target was used to produce nuclides with mass numbers $A = 85$ and 86, whereas enriched target material of ^{54}Fe was optimal for the synthesis of $A = 81$ isotopes. The fine tuning of the primary beam energy was performed with degraders of Havar foil and/or ^{nat}Ni. The reaction products passing through a 2.1 mg/cm^2-thick Havar window were stopped in a helium gas cell of the IGISOL facility [11]. After extraction from the gas cell by helium flow and under a small extraction potential (typically 300 V) the ions were accelerated to 40 keV. The accelerated ion beam was mass-separated and implanted into a collector tape.

The first detector station was situated where the ion beam was implanted into the collector tape (see fig. 4). It consisted of two HPGe detectors situated face-to-face and a plastic scintillator which gated γ-radiation by β-particles. After some time of accumulation at the first station, the tape was moved and the source was delivered to the second detector station where an electromagnetic electron transporter and a low energy Ge detector (LeGe) were installed. The next source was prepared at the first station until the measurements were completed at the second station. Short accumulation and measurement times were optimal for the observation of short-lived nuclei.

Conversion electron decays and low energy gamma radiation were studied at the second detector station. Electron spectra were measured by ELLI [12], a magnetic conversion-electron transporter spectrometer consisting of two coils. It transported electrons from the implantation point to a cooled Si(Au) surface barrier detector in a remote detection area, which helped to reduce the background. A low energy Ge detector with a very thin entrance window (0.5 mm Be) was placed on the opposite side of the Si detector in close geometry with respect to the implantation point (see fig. 4). ELLI had a typical efficiency of about 5 % at electron energies less than 100 keV in this experiment. With this kind of set-up one could measure both the absolute value for α_K and the ratio α_K/α_{L+M}.

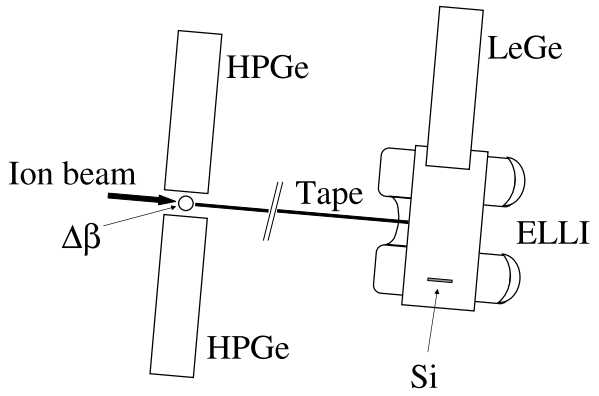

Fig. 4. A schematic view of the detection set-up.

The amplitude and timing data from the detectors were stored event-by-event for subsequent off-line analysis. The energy and efficiency calibrations of the detectors were done with standard sources and with on-line data. Other experimental details are given below in the description of the results.

3 Results

The IGISOL was tuned to obtain optimal yields for short-lived nuclides of interest. Table 1 shows the yields defined as the number of ions per second deposited into the tape at the first detector station. These values represent estimated average yields determined from several individual measurements at different time regimes. Relevant spectroscopic data from literature have been used for the estimations except for a new isomeric state of ^{85}Nb, where a 100 % branching ratio for the internal transition probability was assumed.

Table 1. The yields observed in this work at IGISOL.

Nuclide	$T_{1/2}$	Transitions used	Yield (at/s)
^{81}Zr	5.5 s	γ 113 keV	< 0.2
^{81}Y	70.4 s	γ 79 keV, γ 124 keV	50
^{81}Sr	22.3 min	γ 147.8 keV, γ 186 keV	750
^{81m}Kr	13.1 s	γ 190.5 keV	15
^{85}Nb	20.9 s	γ+e 50 keV	2
^{85m}Nb	3.3 s	e 69 keV	1
^{85}Zr	7.86 min	γ 416 keV, γ 455 keV	200
^{85m}Zr	10.9 s	γ 292.2 keV	5
^{86}Mo	19.6 s	γ+e 47 keV, γ+e 50 keV	15
^{86}Nb	88 s	γ 752 keV, γ 915 keV	25

The main results presented in this chapter concern the analysis of spectra measured at the second detector station which had some important advantages: the detectors were far from the implantation point of the ion beam offering clean conditions and the decay behaviour could be measured properly. The first detector station was used for cross-checking purposes and for the tuning of the installation during the run. The experimental results related to specific mass numbers are presented below.

3.1 Mass A=81

Accumulation times of 15 s and 30 s were used for the measurements at this mass. A part of the low energy γ-spectrum is shown in fig. 5. The most intense peaks used for the yield determination can be seen in this clean spectrum which has no contaminants from neighbouring masses.

An internal conversion electron spectrum is shown in fig. 6. K- and L-electron lines have been identified for known transitions and the 63.1 keV K-electron peak of the 79.2 keV transition in ^{81}Sr has been used for internal calibration. Conversion electrons from 43.0 keV and 221.0 keV transitions in ^{81}Sr have been observed for the first time. The internal conversion coefficient for the 43.0 keV transition has been determined as $\alpha_K = 1.5 \pm 0.3$ which supports an $M1 + E2$ multipolarity for the transition.

Strong lines belonging to a 190.5 keV isomeric transition in ^{81}Kr can be observed in γ- and electron spectra (see figs. 5 and 6). The measured α_K-value is in agreement with the only existing experimental value [13] shown in fig. 7. The experimental values of the ratio α_K/α_{L+M} ([14]-[17]) have been controversial before this experiment, as can be seen in fig. 8. Hereafter, we have used the latest internal conversion coefficient tables [18] for the multipolarity determination. Our values, $\alpha_K = 0.50 \pm 0.07$ and

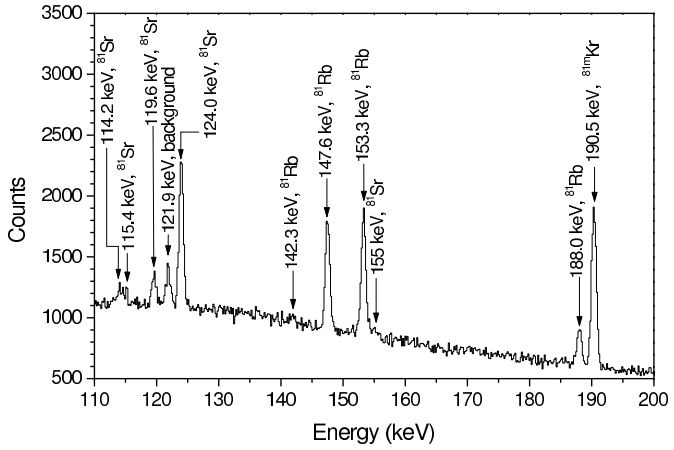

Fig. 5. A low energy part of a γ-spectrum for $A = 81$ measured by the LeGe-spectrometer. The peaks are labelled according to the transitions in daughter nuclei.

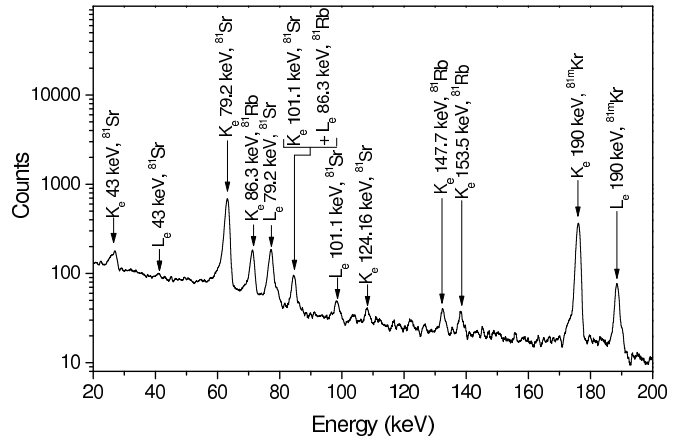

Fig. 6. Internal conversion spectrum measured by the ELLI-spectrometer for the mass number $A = 81$.

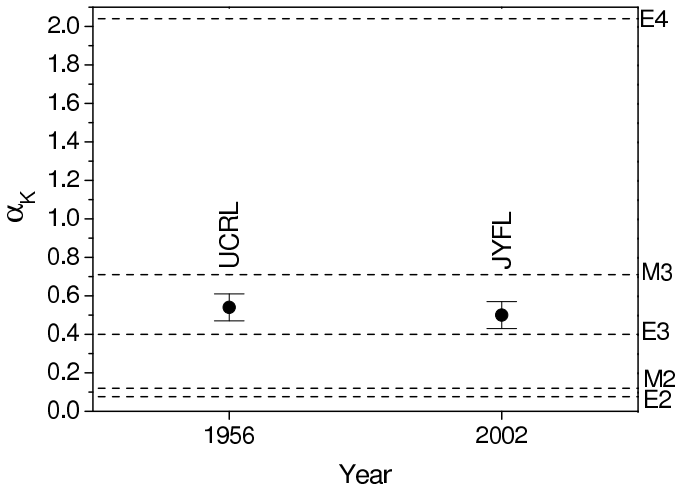

Fig. 7. K-internal conversion coefficient of the 190.5 keV isomeric transition in ^{81}Kr measured in this work in comparison with the value from ref. [13]. The dashed lines show the theoretical values [18].

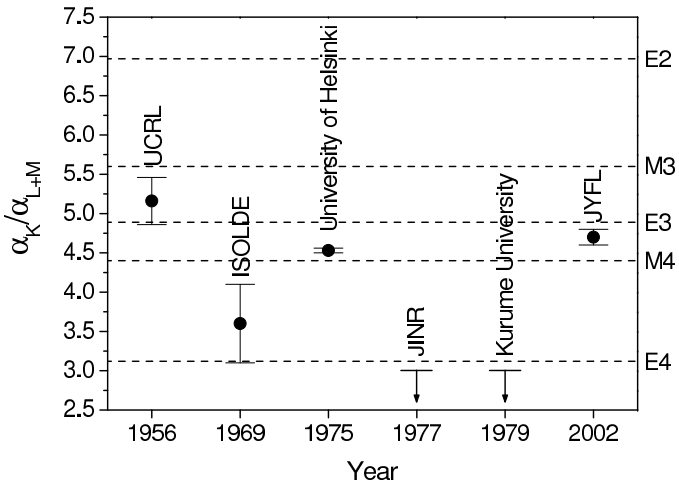

Fig. 8. The values of α_K/α_{L+M} for the 190.5 keV isomeric transition in ^{81}Kr from literature [8] and the one measured in this work. The dashed lines show the theoretical values [18].

$\alpha_K/\alpha_{L+M} = 4.7 \pm 0.1$, favour an $E3$-character for this transition. To check the identification of the ^{81m}Kr line we have determined its half-life, which is shown in fig. 9 for γ- and e^--decay channels. Our average value of 13.4 ± 0.7 s agrees well with the earlier value of 13.10 ± 0.03 s [8].

3.2 Mass A=85

Accumulation times of 15 s and 40 s allowed us to select nuclides with half-lives of seconds and minutes. Indeed, γ- and electron peaks belonging to the decays of ^{85}Nb (21 s), ^{85}Zr (7.9 min) and ^{85m}Zr (10.9 s) were observed. K-conversion electrons with an energy of 32.1 keV corresponding to a 50.1 keV transition in ^{85}Zr can be seen in fig. 10, which shows a spectrum of low energy conversion electrons measured during the first eight seconds of each measurement cycle. This transition from the first excited state to the ground state is the only transition previously observed in the decay of ^{85}Nb [19]. We confirm the identification because the 32.1 keV electron transition is in coincidence with Zr K X-rays. The decays of this electron peak and the corresponding γ-transition are characterised by a half-life of 17 ± 2 s which is little less than the value 20.9 ± 0.7 s attributed to ^{85}Nb in ref. [20] (see fig. 11). Internal conversion coefficients for the observed transitions have been determined for the first time (see table 2). The data suggest an $M1 + E2$ mixture of multipolarities for the 50 keV transition.

An electron line with an energy of 50 keV in fig. 10 cannot be attributed to any known transition in the isobaric mass chain $A = 85$. The coincidence of the 50 keV electrons with the Nb K X-rays (see fig. 12) manifests that this electron line belongs to an unknown transition with an energy of 69 keV in ^{85}Nb. The measured half-life of the transition is 3.3 ± 0.9 s (see fig. 13). According to table 2 the preferable multipolarity for the transition is

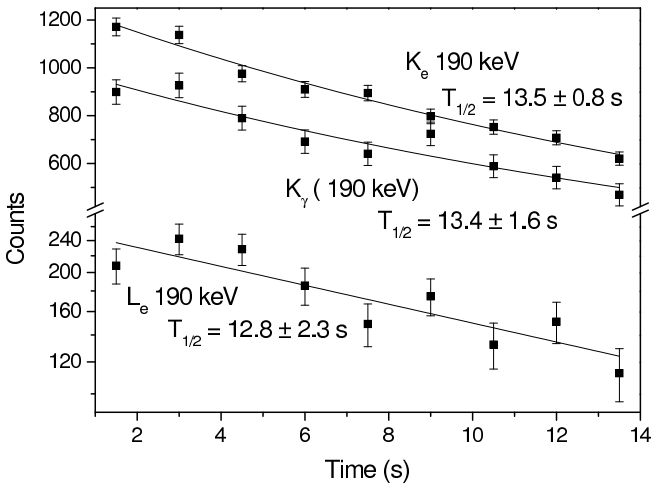

Fig. 9. Time dependent areas for different peaks of the isomeric transition of ^{81m}Kr. The determined half-lives are indicated near the corresponding lines.

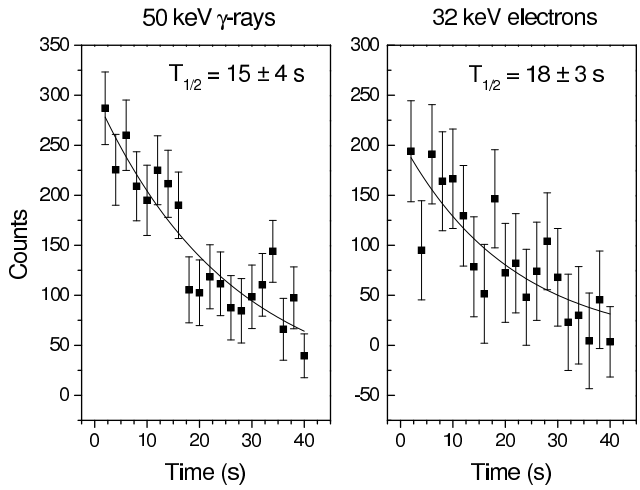

Fig. 11. The time behaviour of γ-rays and conversion electrons from the 50 keV transition in ^{85}Zr. The average half-life of 17 $\pm$ 2 s is little less than the value 20.9 $\pm$ 0.7 s given in ref. [20].

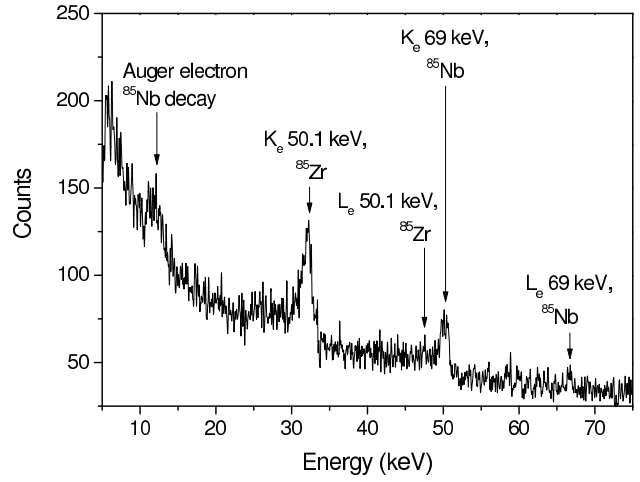

Fig. 10. Internal conversion spectrum measured during the first 8 s of each measurement cycle at mass $A = 85$.

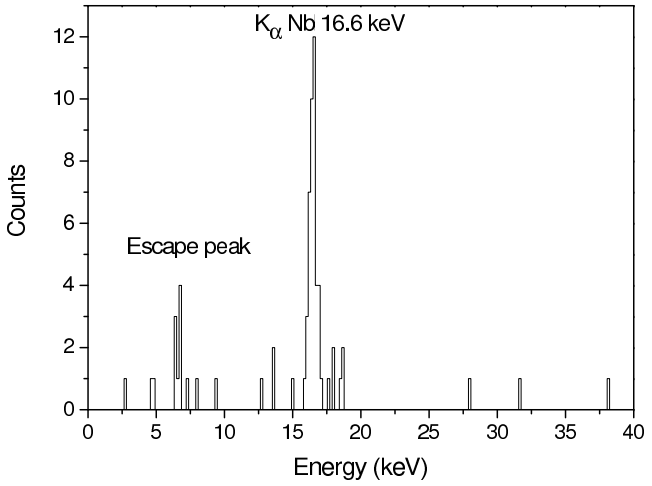

Fig. 12. A low-energy part of the γ-spectrum in coincidence with the electrons of the 69 keV isomeric transition in ^{85}Nb.

$E2$ or $M2$, which cannot solely explain the half-life of the transition.

The new 69 keV transition can originate either from the β^+ decay of ^{85}Mo or from a decay of a new isomeric state in ^{85}Nb. Further analysis showed that there is no coincidence of this peak with the annihilation radiation, which supports the latter option. In addition, the yield of this new transition is 0.8 transitions/s which is similar to the yield of ^{85}Nb ground state (2 ions/s) shown in table 1. We can also note that the yield ratio for ^{85}Mo/^{85}Nb in reaction ^{32}S+^{nat}Ni should be approximately the same as the yield ratio for ^{81}Zr/^{81}Y in the reaction ^{32}S+^{54}Fe, which is less than 0.4 % (see table 1). This gives an upper limit of 0.01 ions/s for the expected yield of ^{85}Mo, which disagrees strongly with the observed yield of the new transition and speaks in favour of the identification of ^{85m}Nb. Figure 14 shows a proposed decay scheme of ^{85}Nb.

We have also observed a γ-transition with an energy of 292 keV belonging to a known isomeric state, ^{85m}Zr. Conversion electrons from this transition could not be observed since their energy was above the maximum energy detected by the ELLI detector. The measured half-life of 12 $\pm$ 2 s for this state is consistent with the average value of 10.9 $\pm$ 0.3 s from ref. [19]. An indication of beta decay from ^{85m}Nb to the 292 keV state of ^{85m}Zr has also been observed in the time behaviour of the 292 keV transition (see fig. 15). As the spin of the 292 keV state is tentatively $1/2^-$ [19], allowed beta transition suggests spins of $1/2^-$ or $3/2^-$ for ^{85m}Nb (see fig. 14).

3.3 Mass A=86

In order to observe both ^{86}Mo and ^{86}Nb, accumulation times of 40 s and 200 s were used. Gamma lines with energies of 47.7 keV and 50.1 keV as well as Nb and Zr K X-rays can be seen in γ-spectrum gated by electrons (see fig. 16). These gamma peaks belong to a cascade de-excitation of the E_0+97.1 keV level in ^{86}Nb [22] which is

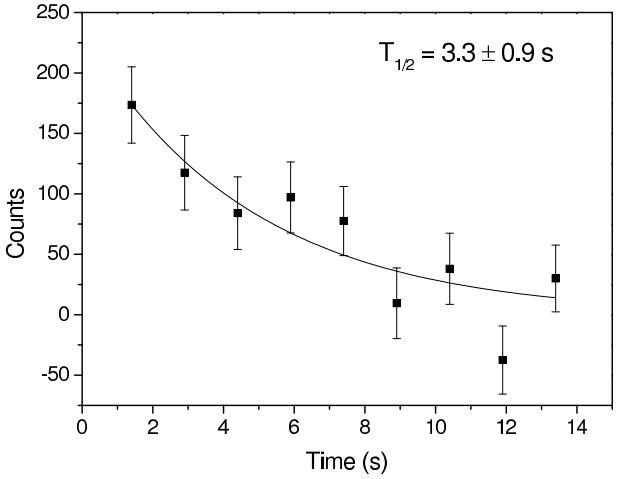

Fig. 13. Background-corrected conversion electron intensities as a function of time for the 69 keV transition in ^{85}Nb.

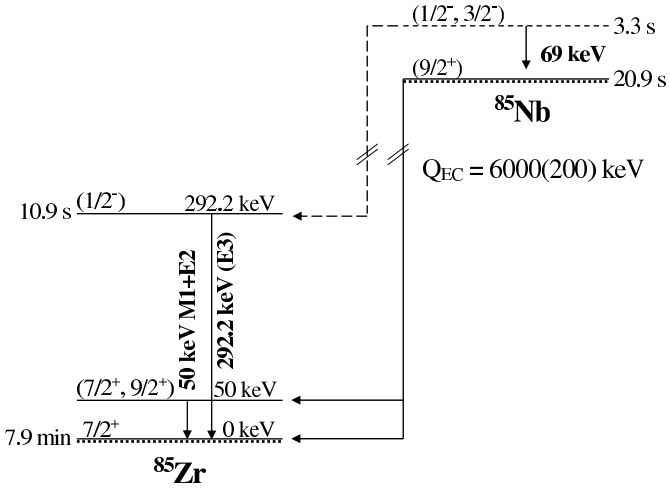

Fig. 14. A proposed decay scheme of ^{85}Nb. The Q-value is taken from ref. [21] and the suggested multipolarity $E3$ is from ref. [19].

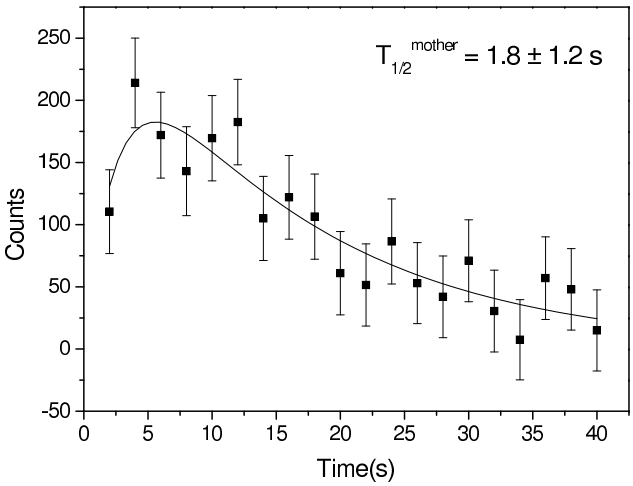

Fig. 15. A fit on the time behaviour of the 292 keV γ-transition of ^{85m}Zr (normalised $\chi^2 = 0.50$) assuming that the state is fed from a mother nucleus and the half-life of ^{85m}Zr is fixed to 10.9 s [19]. A half-life of 1.8 ± 1.2 s obtained for the mother nuclide agrees with the half-life of ^{85m}Nb. An exponential decay fit on the decay part yields a half-life of 12 ± 2 s for ^{85m}Zr.

Table 2. Internal conversion coefficients (α_K) and intensity ratios of K and L peaks (I_K/I_L) for $A = 85$ nuclei.

γ-transition	α_K (exp.)	α_K (theor.)	I_K/I_L (exp.)	I_K/I_L (theor.)
50 keV ^{85}Zr	1.7±0.2	0.75 ($E1$)	9.0±1.8	8.1 ($E1$)
		1.3 ($M1$)		8.1 ($M1$)
		9.8 ($E2$)		2.8 ($E2$)
		23.7 ($M2$)		5.2 ($M2$)
69 keV ^{85}Nb	> 2.6	0.31 ($E1$)	4.1±1.3	7.15 ($E1$)
		0.57 ($M1$)		7.0 ($M1$)
		3.43 ($E2$)		3.0 ($E2$)
		7.83 ($M2$)		3.86 ($M2$)
		29.7 ($E3$)		1 ($E3$)
		83 ($M3$)		2.54 ($M3$)

fed by the beta decay of ^{86}Mo [23]. The cascade nature is supported by strong coincidences between the electrons from one of the 47.7 keV and 50.1 keV transitions and the γ-line of the other transition (see fig. 17). A new peak with an energy of 97.8 keV is also observed in fig. 16. This transition has no coincidence with the cascade peaks and could be considered as a crossover transition from the level with an energy of E_0+97.8 keV in ^{86}Nb.

Conversion coefficients listed in table 3 support an $M1$ character for the 47.7 keV transition and $E1$ for the 50.1 keV transition. The multipolarities for the 97.8 keV and 186.8 keV transitions are most likely $E1$. The 186.8 keV transition populates the level at E_0+50.1 keV because it is in coincidence only with the electron line belonging to the 50.1 keV transition. The decay scheme is shown in fig. 18. The spin identifications are different from [23], where the $M1$ multipolarity was given for the 50 keV transition instead of $E1$ and the multipolarity of the 187 keV transition was not determined. The position of the level E_0 is still unknown.

The half-life of ^{86}Mo has been determined from the time behaviour of γ-, Nb K X-ray and electron peaks. The weighted average value is 19.1 ± 0.3 s confirming the half-life of 19.6 ± 1.1 s obtained in [23]. No indication of the existence of an isomer in ^{86}Nb with a half-life of 56 s [23] has been observed.

4 Discussion

Nuclei with mass numbers $A = 81, 85$ and 86 are particularly interesting because the short-lived exotic members of these isobaric chains are situated at the rp-process path (see fig. 1). We have concentrated on specific nuclei of astrophysical importance, such as ^{85}Nb, which is involved in the proton capture process. The observation of a new isomer with a half-life of 3.3 s in ^{85}Nb should be taken

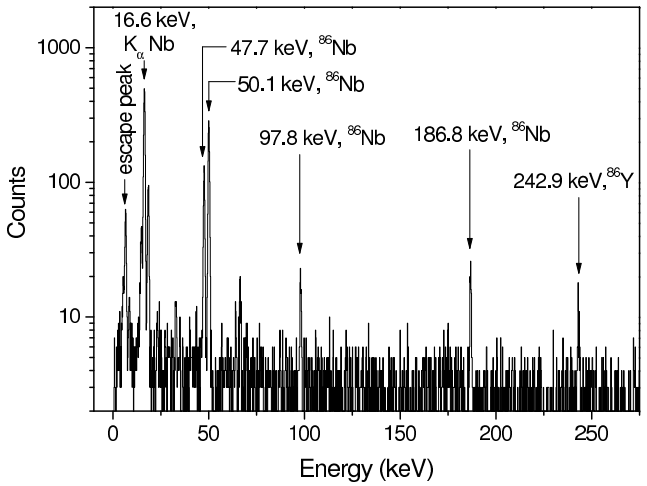

Fig. 16. A γ-ray spectrum measured by the LeGe-detector gated by electrons at mass $A = 86$. The peaks are labelled according to the transitions in daughter nuclei.

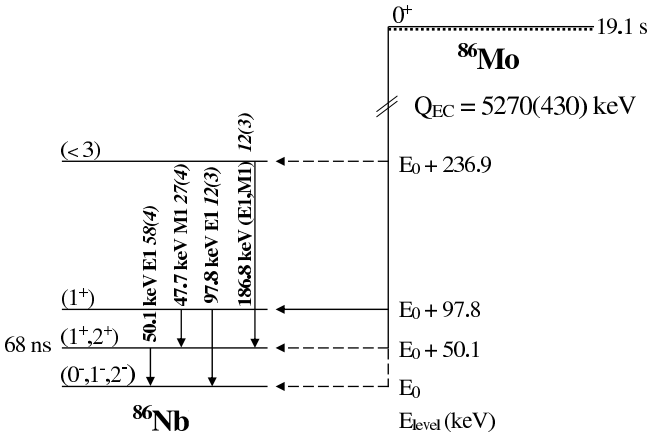

Fig. 18. A proposed decay scheme of ^{86}Mo. The γ-intensities are normalised by the 50.1 keV transition. The Q-value is taken from ref. [21].

into account in the rp-process network calculations. An isomer in ^{85}Nb was expected from the systematics of odd-A Nb isotopes between ^{89}Nb and ^{99}Nb all of which have a $9/2^+$ ground state and a low-lying $1/2^-$ isomeric state (see fig. 19). These states can be explained by an extreme single-particle shell-model as having an odd proton in a $1g_{9/2}$ or in a $2p_{1/2}$ orbital.

The measured internal conversion coefficients propose an $E2$ or $M2$ multipolarity for the 69 keV transition in ^{85}Nb. However, the calculated Weisskopf estimates for the half-life ($T_{1/2}(E2) = 1.6 \times 10^{-5}$ s, $T_{1/2}(M2) = 1.0 \times 10^{-3}$ s, $T_{1/2}(E3) = 380$ s and $T_{1/2}(M3) = 2.4 \times 10^4$ s) suggest that the transition could be $M2$ with a significant mixture of $E3$. Another explanation for the observed half-life is that the isomeric state decays by a low energy transition which feeds the 69 keV transition. If this is the case, that highly converted transition could not have been observed in coincidence with the electrons from the 69 keV transition.

The half-lives and isomeric level structures of ^{86}Mo and ^{86}Nb are of potential astrophysical relevance as during freezeout they can impact the final distribution of isotopic abundances in the $A = 86$ mass region produced by the rp-process. We have confirmed the half-life of ^{86}Mo [23], but we did not observe an isomeric state with a half-life of 56 s in ^{86}Nb claimed in ref. [23]. The existence of this isomer has already been considered as uncertain due to a possible mixed activity of the 88 s, (6^+) isomer and a low-spin isomer of unknown half-life populated in ^{86}Mo EC decay [22]. We have not seen any converted transition from the state with an unknown energy E_0 in ^{86}Nb. Therefore, we can conclude that either this state is highly excited and decays by a high energy transition or the main channel of de-excitation is the direct β^+ decay to the states in ^{86}Zr.

The beta decay scheme of ^{86}Mo and the de-excitation scheme of the excited states in ^{86}Nb obtained in this work change the spin identification of the isomeric state E_0 from

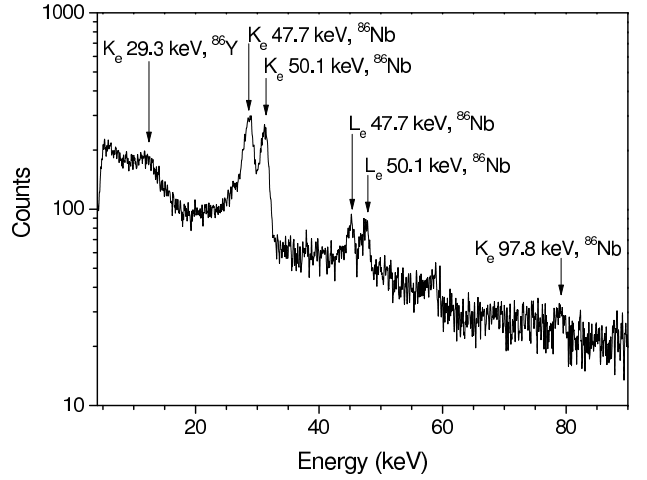

Fig. 17. A part of the internal conversion electron spectrum measured by the ELLI-spectrometer at mass $A = 86$.

Table 3. Internal conversion coefficients (α_K) and intensity ratios of K, L and M peaks (I_K/I_{L+M}) for the mass number $A = 86$.

E_γ (keV)	α_K (exp.)	α_K (theor.)	I_K/I_{L+M} (exp.)	I_K/I_{L+M} (theor.)
47.7	1.8±0.3	0.89($E1$)	8.3±0.7	8.3($E1$)
		1.64($M1$)		8.4($M1$)
		11.4($E2$)		2.6($E2$)
		31.6($M2$)		5.1($M2$)
50.1	0.65±0.10	0.77($E1$)	6.5±0.6	8.3($E1$)
		1.4($M1$)		8.4($M1$)
		9.8($E2$)		2.8($E2$)
		26.2($M2$)		5.2($M2$)
97.8	0.09±0.04	0.11($E1$)	-	-
		0.21($M1$)		
186.8	< 0.04	0.017($E1$)	-	-
		0.0036($M1$)		

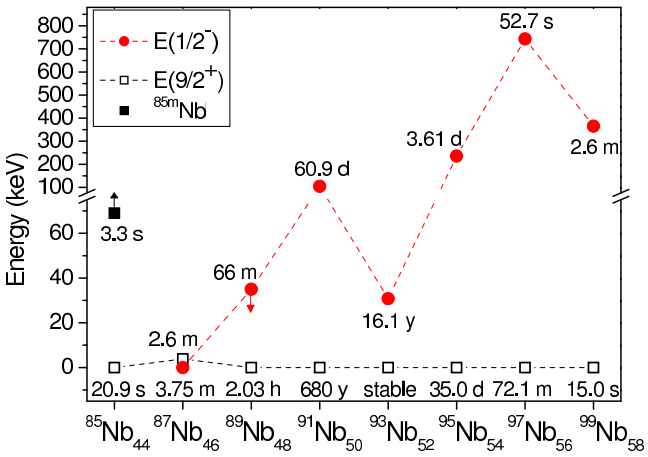

Fig. 19. Isomeric states in odd-A Nb isotopes taken from refs. [19] and [24]– [30] for $A = 85$–99, respectively. The half-lives are marked next to the states. Spin and parity assignments are not certain for ^{85}Nb, ^{87}Nb and ^{89}Nb. The arrows show lower or upper limits for the states.

ref. [23], where $M1$ multipolarity was given for the 50 keV transition instead of $E1$. The new spin assignment implies that the beta decay to the E_0 level should be weak. For the levels at E_0+50.1 keV, E_0+97.8 keV and E_0+236.9 keV log ft values between 4.5 and 5.0 have been estimated assuming $Q_{EC} = 5270 \pm 430$ keV [21] for the E_0 level and negligible beta decay branchings to other levels. A spin less than 3 is expected from the log ft estimate for the state at E_0+236.9 keV.

Another application of our data in astrophysics concerns the proposed ^{81}Br neutrino detector for which the decay properties of ^{81m}Kr are crucial. The electron capture branching ratio η_ε of the isomeric state ^{81m}Kr, which is inverse to the neutrino capture process (see fig. 3), can be deduced from the relation:

$$\eta_\varepsilon = \frac{\lambda_\varepsilon}{\lambda_e + \lambda_\gamma + \lambda_\varepsilon} = \frac{\lambda_{\varepsilon_K}\left(1 + \frac{\lambda_{(\varepsilon_L+\varepsilon_M)}}{\lambda_{\varepsilon_K}}\right)}{\lambda_{e_K}\left(1 + \frac{\lambda_{(\varepsilon_L+\varepsilon_M)}}{\lambda_{e_K}}\right)\left(1 + \frac{\lambda_\gamma}{\lambda_e}\right) + \lambda_{\varepsilon_K}\left(1 + \frac{\lambda_{(\varepsilon_L+\varepsilon_M)}}{\lambda_{\varepsilon_K}}\right)} \quad (1)$$

where λ_e, λ_γ and λ_ε stand for internal conversion, gamma transition and electron capture probabilities, respectively. Indices K, L and M label the corresponding atomic shells.

If $\eta_\varepsilon \ll 1$, as it is expected for the decay of ^{81m}Kr, we can deduce the following expression:

$$\eta_\varepsilon = \left(1 + \frac{\lambda_{(\varepsilon_L+\varepsilon_M)}}{\lambda_{\varepsilon_K}}\right) \times \frac{K_X(Br)\omega_K(Kr)}{K_X(Kr)\omega_K(Br)} \times \frac{\alpha_K}{(1+\alpha_{tot})} \quad (2)$$

where K_X is the intensity of characteristic X-rays corresponding to the K-shell, ω_K stands for the respective K-fluorescence yield and α represents the internal conversion coefficient. As a summary, the electron capture branching ratio depends on the following factors:

Table 4. Neutrino capture probability for the ^{81}Br $\rightarrow$ ^{81m}Kr transition.

Group	Argonne [10]	Princeton [9]	This work
η_ε ($\times 10^{-5}$)	3.14 ± 0.58	2.26 ± 0.32	-
Average η_ε ($\times 10^{-5}$)	2.47 ± 0.37		3.0 ± 0.5
α_K	0.4	0.4	0.50 ± 0.07
α_{tot}	0.48	0.49	0.61 ± 0.09
log ft (ν capture)	5.19 ± 0.07		5.13 ± 0.09

– the ratio of electron capture branches $\lambda_{(\varepsilon_L+\varepsilon_M)}/\lambda_{\varepsilon_K}$
– the intensity ratio of Br K X-rays to Kr K X-rays
– the ratio $\alpha_K/(1+\alpha_{tot})$

We have now calculated the first factor with the values from ref. [31] and taken into account overlapping and exchange effects [32], which will lead to $\lambda_{(\varepsilon_L+\varepsilon_M)}/\lambda_{\varepsilon_K} = 0.144$. Groups at Princeton [9] and Argonne [10] have considered the second factor and measured the ratio for K X-rays. However, in order to determine the electron capture branching ratio η_ε, they used theoretical values for the estimation of the first factor ($\lambda_{(\varepsilon_L+\varepsilon_M)}/\lambda_{\varepsilon_K} = 0.119$) and for internal conversion coefficients ($\alpha_K = 0.4$ and $\alpha_{tot} = 0.48$). In the present work we have measured the internal conversion coefficients needed for the third factor, $\alpha_K/(1+\alpha_{tot})$.

The experimental values for internal conversion coefficients and for the intensity ratio of K X-rays [9,10] together with a revised value for the ratio of electron capture branches were used to compute the neutrino capture rate of the $3/2^- \rightarrow 1/2^-$ transition in the ^{81}Br detector. The corresponding log ft value calculated with the tabulated f-values from [31] is given in table 4 in comparison with the averaged value taken from [8]. Our value is slightly lower than the earlier value leading to an increased neutrino capture cross section. This supports the conclusion that ^{81}Br can be successfully used as a solar neutrino flux detector.

5 Conclusions

We have investigated decay properties of nuclei close to the $N = Z$ line at the rp-process path at masses $A = 81, 85$ and 86. As the half-lives of the nuclides in this area are typically known only from single measurements we have remeasured and confirmed them. A new isomeric state with a half-life of 3.3 s has been identified in ^{85}Nb. We could not confirm the existence of an isomeric state with a half-life of 56 s in ^{86}Nb. The investigation of both γ- and electron channels shows that the spin identification of the state E_0 in ^{86}Nb should be changed from the assignment used in [23]. The implementation of our new results into astrophysical rp-process models will require the calculation of thermalisation timescales and proton capture

rates on excited states for a range of rp-process conditions. This is beyond the scope of the present work.

The measured electron and γ-decay branches for the 190.5 keV isomeric transition in ^{81m}Kr (13.1 s) allowed the estimation of a new branching ratio for electron capture of the isomeric state considered as a daughter nuclide in the neutrino capture process on the ^{81}Br neutrino detector. Our experimental data on the internal conversion coefficient for this transition provided new information about the decay rates, which were very contradictory thus far. The recalculated neutrino-capture rate is slightly higher than previously claimed.

This work has been supported by the European Union Fifth Framework Programme "Improving Human Potential - Access to Research Infrastructure"(Contract No. HPRI-CT-1999-00044) and by the Academy of Finland under the Finnish Centre of Excellence Programme 2000-2005 (Project No. 44875, Nuclear and Condensed Matter Physics Programme at JYFL). H.S. acknowledges support through NSF grants PHY-0110253 and PHY-0216783 (Joint Institute for Nuclear Astrophysics).

This work has been performed within the framework of Agreement between Finnish and Russian Academies (the Project No. 8). Russian participants are grateful to the Russian Academy for support and to the Finnish Academy and the Accelerator Laboratory of University of Jyväskylä for support and warm hospitality. Finally, we would like to thank M.B. Trzhaskovskaya for fruitful discussions.

References

1. H. Schatz *et al.*, Phys. Rep. **294**, 167 (1998).
2. H. Schatz *et al.*, Nucl. Phys. A **688**, 150c (2001).
3. Yu.N. Novikov *et al.*, Eur. Phys. J. A **11**, 257 (2001).
4. R. Davis *et al.*, Phys. Rev. Lett. **20**, 1205 (1968).
5. R.D. Scott, Nature **264**, 729 (1976).
6. J.N. Bahcall *et al.*, Phys. Rev. Lett. **90**, 131301 (2003).
7. D. Krofcheck *et al.*, Phys. Lett. B **189**, 299 (1987).
8. C.M. Baglin, Nucl. Data Sheets **79**, 447 (1996).
9. M.M. Lowry *et al.*, Phys. Rev. C **35**, 1950 (1987).
10. C.N. Davids *et al.*, Phys. Rev. C **35**, 1114 (1987).
11. J. Äystö, Nucl. Phys. A **693**, 477 (2001).
12. J.M. Parmonen *et al.*, Nucl. Instr. Meth. A **306**, 504 (1991).
13. W.O. Doggett, Lawrence Radiation Laboratory Report No. UCRL-3438, 1956, unpublished.
14. P.G. Hansen *et al.*, Phys. Lett. **28B**, 415 (1969).
15. S. Väisälä *et al.*, Phys. Fenn. **10**, 133 (1975).
16. J. Lipták *et al.*, Nucl. Phys. A **286**, 263 (1977).
17. K. Toyoshima, Nucl. Phys. A **323**, 61 (1979).
18. I.M. Band *et al.*, Atom. Data and Nucl. Data Tables **81**, 1 (2002).
19. H. Sievers, Nucl. Data Sheets **62**, 271 (1991).
20. T. Kuroyanagi *et al.*, Nucl. Phys. A **484**, 264 (1988).
21. G. Audi *et al.*, Nucl. Phys. A **729**, 337 (2003).
22. B. Singh, Nucl. Data Sheets **94**, 1 (2001).
23. T. Shizuma *et al.*, Z. Phys. A **348**, 25 (1994).
24. R.G. Helmer, Nucl. Data Sheets **95**, 543 (2002).
25. B. Singh, Nucl. Data Sheets **85**, 1 (1998).
26. C.M. Baglin, Nucl. Data Sheets **86**, 1 (1999).
27. C.M. Baglin, Nucl. Data Sheets **80**, 1 (1997).
28. T.W. Burrows, Nucl. Data Sheets **68**, 635 (1993).
29. A. Artna-Cohen, Nucl. Data Sheets **70**, 85 (1993).
30. L.K. Peker, Nucl. Data Sheets **73**, 1 (1994).
31. B.S. Dzhelepov *et al.*, *Beta processes, Functions for the analysis of beta spectra and electron capture* (Nauka, Leningrad, 1972).
32. A. Faessler *et al.*, Z. Phys. A **238**, 352 (1970).